Near-infrared double negative metamaterials

Shuang Zhang, Wenjun Fan, K. J. Malloy and S. R. J. Brueck

Center for High Technology Materials, University of New Mexico, Albuquerque, NM 87106
brueck@chtm.unm.edu

N. C. Panoiu and R. M. Osgood

Department of Applied Physics and Applied Mathematics, Columbia University, New York, NY 10027

Abstract: We numerically demonstrate a metamaterial with both negative ε and negative μ over an overlapping near-infrared wavelength range resulting in a low loss negative-index material. Parametric studies optimizing this negative index are presented. This structure can be easily fabricated with standard semiconductor processing techniques.

OCIS codes: (260.2030) Physical optics; (290.3030) Scattering; (310.6860) Thin films

Reference and links

1. R. A. Shelby, D. R. Smith, S. Schultz, "Experimental Verification of a Negative Index of Refraction," Science **292**, 77-79 (2002).
2. J. B. Pendry, "Negative refraction makes a perfect lens," Phys. Rev. Lett. **85**, 3966-3969 (2000).
3. N. C. Panoiu and R. M. Osgood, "Influence of the dispersive properties of metals on the transmission characteristics of left-handed materials," Phys. Rev. E **68,** 016611(2003).
4. N. C. Panoiu and R. M. Osgood, "Numerical investigation of negative refractive index metamaterials at infrared and optical frequencies," Opt. Commun. **233**, 331 (2003).
5. T. J. Yen, W. J. Padilla, N. Fang, D. C. Vier, D. R. Smith, J. B. Pendry, D. N. Basov, and X. Zhang, "Terahertz Magnetic Response from Artificial Materials,**"** Science **303**, 1494-1496 (2004)
6. Stefan Linden, Christian Enkrich, Martin Wegener, Jiangfeng Zhou, Thomas Koschny, and Costas M. Soukoulis, "Magnetic Response of Metamaterials at 100 Terahertz,**"** Science **306**, 1351-1353 (2004).
7. Shuang Zhang, Wenjun Fan, A. Frauenglass, B. Minhas, K. J. Malloy and S. R. J. Brueck, "Demonstration of Mid-Infrared Resonant Magnetic Nanostructures Exhibiting a Negative Permeability," Phys. Rev. Lett. **94**, 037402 (2005).
8. Shuang Zhang, Wenjun fan, N. C. Panoiu, K. J. Malloy, R. M. Osgood, S. R. J. Brueck, "Demonstration of Near-Infrared Negative-Index Materials," Postdeadline Paper at OSA Topical Meeting on NanoPhotonics for Information Systems (April 15, 2005), at IQEC (May 26, 2005) and submitted to Phys. Rev. Lett. Also available at: http://arxiv.org/ftp/physics/papers/0504/0504208.pdf (2005)
9. Vladimir M. Shalaev, Wenshan Cai, Uday Chettiar, Hsiao-Kuan Yuan, Andrey K. Sarychev, Vladimir P. Drachev, Alexander V. Kildishev, "Negative Index of Refraction in Optical Metamaterials," http://arxiv.org/ftp/physics/papers/0504/0504091.pdf. (2005)
10. M. G. Moharam and T.K. Gaylord, "Rigorous coupled-wave analysis of planar-grating diffraction," J. Opt. Soc. Am. 71, 811-818 (1981).
11. B. K. Minhas, W. Fan, K. Agi, S. R. J. Brueck and K. J. Malloy, "Metallic Inductive and Capacitive Grids: Theory and Experiment," J. Opt. Soc. Am. **A19**, 1352-1359 (2002).
12. D. R. Smith and S. Schultz, "Determination of effective permittivity and permeability of metamaterials from reflection and transmission coefficients," Phys. Rev. **B65**, 195104. (2002)
13. S. O'Brien and J. B. Pendry, "Magnetic activity at infrared frequencies in structured metallic photonic crystals," J. Phys. Condens. Matter **14**, 6383-6394 (2002).
14. M. Qui, "Effective Index Method for Heterostructure-Slab-Waveguide-Based Two-Dimensional Photonic Crystals," Appl. Phys. Lett. **81**, 1163-1165 (2002).
15. J. H. Weaver, C. Krafka, D. W. Lynch and E. E. Koch, *Optical Properties of Metals, Physics Data Vols. I and II* (Fachinformationzentrum, Karlsrube, Germany, 1981), Vol. 18-2.
16. M.K. Karkkainen, "Numerical study of wave propagation in uniaxially anisotropic Lorentzian backward-wave slabs," Phys. Rev. **E68**, 026602 (2003).
17. J. B. Pendry, L. Martin-Moreno and F. J. Garcia-Vidal, "Mimicking Surface Plasmons with Structured Surfaces," Science **305**, 847-848 (2004).
18. Xiaolan Chen, Saleem H. Zaidi, S. R. J. Brueck and D. J. Devine, "Interferometric Lithography of Sub-Micrometer Sparse Hole Arrays for Field-Emission Display Applications," J. Vac. Sci. Technol. **B14**, 3339-3349 (1996).

#7325 - $15.00 USD Received 29 April 2005; revised 10 June 2005; accepted 13 June 2005

1. Introduction

Since the experimental demonstration of a negative index material (NIM) in the microwave region [1] and the discussion of the potential application of NIM as a lens beyond the diffraction limit [2], much effort has been put into investigating negative-index metamaterials in the near-infrared (NIR) and visible wavelength regions where simple scaling of the structures used for RF NIMs is difficult [3, 4]. Recently, several experiments have demonstrated a negative permeability in the THz and mid-infrared regions [5-7].

To obtain negative refraction, both magnetic and electric responses (permeability and permittivity) need to be controlled over an overlapping wavelength range. Two recent reports have demonstrated the fabrication and characterization of a NIR negative refractive index material [8, 9]. In Ref. [8], the negative index material consists of a pair of gold films separated by a dielectric layer with a two-dimensional, square-periodic array of circular holes perforating the entire multilayer structure. The magnetic resonance between the two gold films along with the electric response of the gold film to the external electrical field results in the negative refraction for propagation normal to the films. The negative refractive index was obtained at a wavelength around 2 μm; the real part is as negative as –2 and the imaginary part is about +3. The imaginary part of the index being larger than the real part indicates significant loss, which is also the case for reference [9].

The refractive index is expressed in terms of the real and imaginary parts of the permittivity and permeability as $n \equiv n_1 + in_2 = \sqrt{(\varepsilon_1\mu_1 - \varepsilon_2\mu_2) + i(\varepsilon_1\mu_2 + \varepsilon_2\mu_1)}$, where $\varepsilon = \varepsilon_1 + i\varepsilon_2$ and $\mu = \mu_1 + i\mu_2$. To achieve a negative n_1, the imaginary part inside the square root needs to be < 0, which can be satisfied for a sufficiently large imaginary term without requiring both ε_1 and μ_1 to be negative. In Ref. [8], at the wavelength with negative index, ε_1 is negative and large, $\varepsilon_1 >> \varepsilon_2$, giving, $n \approx \sqrt{\varepsilon_1\mu_1 + i\varepsilon_1\mu_2}$. Around the magnetic resonance, $\mu_2 > 0$, which indicates that the real part of n is negative even if $\mu_1 > 0$. However, the sign of μ_1 determines the relative magnitudes of the imaginary and real parts of the refractive index, with $n_1 > n_2$ for $\mu_1 < 0$, and the opposite for $\mu_1 < 0$. Thus, to achieve a negative index with a small imaginary part of the index, a negative permeability is required. In this paper, we numerically study a structure similar to that in Ref. [8] and demonstrate that a NIR negative index material can be achieved with both negative ε_1 and μ_1, and thus a reduced loss.

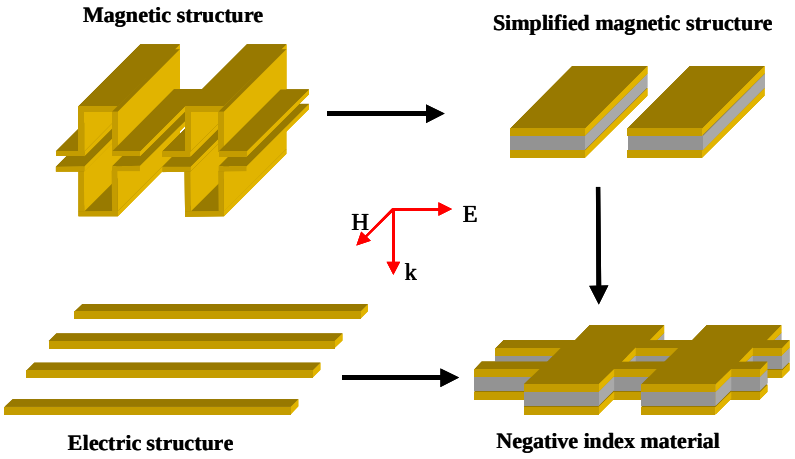

Fig. 1. Schematic of the NIM design (a) Staple structures for magnetic resonance (Ref. 7) (b) A simplified structure for magnetic resonance. (c) Array of metallic wires along the electrical field direction for electrical response. (d) Combining (b) and (c) to get a negative index material.

#7325 - $15.00 USD
Received 29 April 2005; revised 10 June 2005; accepted 13 June 2005

2. Proposed structure and simulation method

Figure 1(a) shows the schematic of the staple structure exhibiting negative permeability demonstrated in Ref. [7]. This structure is a L-C circuit with an inductance associated with both the loop and the electron inertia, and a capacitance formed by the staple footings. A simplified, higher-frequency version of the staple structure is just a pair of finite-width metal stripes parallel to the direction of magnetic field separated by a dielectric layer (e.g. distributed inductance/capacitance), as shown in Fig.1 (b). It is well known that an array of thin metallic wires along the direction of electrical field can introduce a negative ε [Fig. 1(c)], combining the structures in Figs. 1(b) and 1(c) results in a negative index material with both magnetic and electric responses. A question is to how the incorporation of the thin wires affects the resonance of magnetic structure; this will be studied below by comparing the optical properties of structure shown in Fig. 1(d) (with thin metal wires along the electric field direction) with that in Fig. 1(b) (without the metal wires).

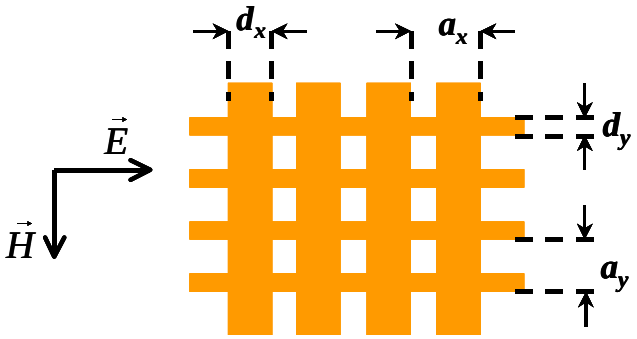

Fig. 2. Top view of the structure with geometrical parameters indicated.

Rigorous coupled-wave analysis (RCWA), a commonly used algorithm to calculate the transmission and reflection of periodic structures, was used for the simulations [10, 11]. For all of the calculations, the incident light is normal to the surface and both the incident and outgoing media are air. Multiple diffraction orders (19) are kept in both directions, which is sufficient to converge very well for all of the simulated structures. The results of the RCWA simulation and the experiment are found to be in very good agreement for a similar structure in Ref. [8]. The geometrical parameters of the structure are indicated in the top view shown in Fig. 2. The pitches of the 2D gratings a_x and a_y are both fixed to 801 nm, less than the resonance wavelength of about 2 μm. The refractive index of the dielectric layer between the gold films is taken to be 1.5. The thicknesses of the Au/dielectric/Au layers are fixed at 30/60/30 nm, respectively. We systematically vary the linewidth of the gratings d_x and d_y in the simulation to study the magnetic and electric response of the structure. After the complex coefficients of transmission and reflection are obtained by RCWA, the effective refractive index and impedance can be extracted following the methods in Ref. [12, 13].

For propagation in the vertical direction (z), the use of an effective-medium model is justified [14] in the presence of a periodic structure in the x-y plane with scales comparable to the wavelength. In our evaluations, the period of 801 nm is significantly smaller than the resonance wavelength of 2 μm. The present calculations are for a single three-layer structure and the dimension of the metamaterial in the z-direction is just the physical thickness of the three layers. In future work, this will be extended to thicker, more complex structures.

3. Simulation results for bulk gold parameters

We first investigate the magnetic resonant structure shown in Fig. 1(b) (e.g. $d_y = 0$). Structures with three different Au grating linewidths (d_x = *400 nm, 500 nm, 600 nm*) were modeled to investigate the effect of the linewidth on the position and strength of the magnetic resonance.

#7325 - $15.00 USD Received 29 April 2005; revised 10 June 2005; accepted 13 June 2005

Bulk gold dispersion parameters were used in the simulation [15]. As shown in Fig. 3, the resonance wavelength increases with the linewidth of Au gratings. This trend can be qualitatively explained by tracking the resonance of an equivalent L-C circuit; a wider grating corresponds to larger inductance and capacitance, which in turn leads to a larger resonance wavelength. As shown in the inset of Fig. 3, the resonance wavelength is linearly dependent on the Au linewidth d_x. An Au linewidth of 500 *nm* (d_x) was used in the simulation of the 2D negative index structures.

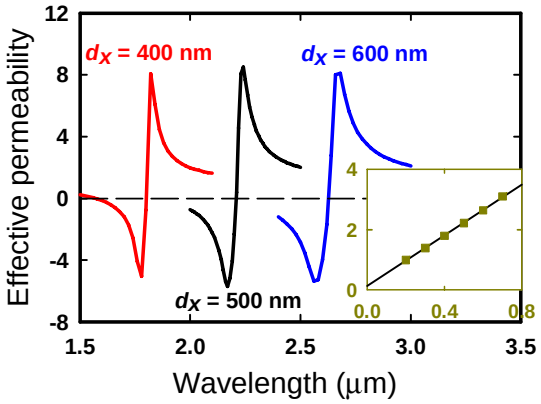

Fig. 3. Effective permeability for different Au linewidths. The inset shows the wavelength of the resonance peak versus the Au linewidth d_x in μm.

The linewidth of the Au gratings along the direction of electric field d_y was varied from 100- to 500-nm and transmission and reflection were calculated. Fig. 4 shows the simulated transmission spectra. With an increase of d_y, the resonance shifts to shorter wavelength, indicating an interaction between the electric and magnetic structures. The transmission decreases (reflection increases) as d_y becomes larger, due to metal polarizer effects. When d_y is small, the resonance is characterized by dip in the transmission, for increasing d_y a peak is clearly formed. The transmission phase exhibits a dip around the resonance, indicating that the light is advanced in phase at the resonance, characteristic of a negative index material.

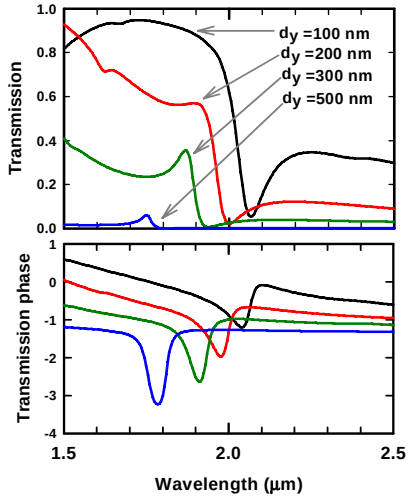

Fig. 4. Top - transmission of samples with different d_y at fixed d_x of 500 nm. The bottom panel shows the transmission phase.

#7325 - $15.00 USD Received 29 April 2005; revised 10 June 2005; accepted 13 June 2005

Using the transmission and reflection simulations, the effective refractive index and impedance can be extracted as shown in Fig. 5(a). The bandwidth of the negative refraction roughly matches the bandwidth of phase dip in Fig. 4. For different d_y parameters, the minimum values of the real part of the refractive index range from about -4 to -6, initially increasing with linewidth, peaking at d_y=*300 nm*, and then decreasing. From Figs. 4 and 5(a), for the sample with d_y = 100 nm, over 80% transmission is obtained over the negative index wavelength range, while for the sample with the largest d_y, only < 10% of the light is transmitted. The impedance of the structure, shown in Fig. 5(b), explains the high transmission for small d_y; the real part of the impedance is closer to the condition for impedance matching (~ 1).

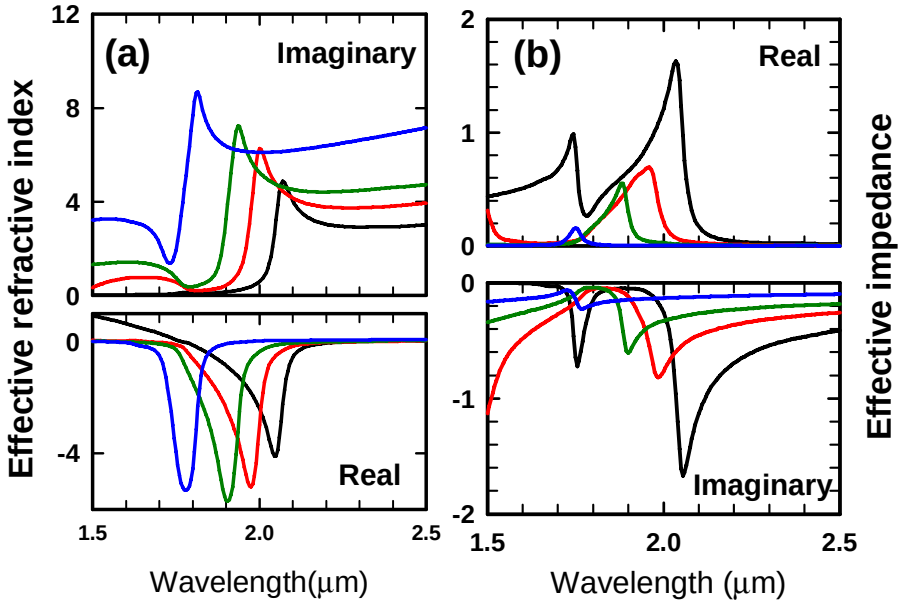

Fig. 5. (a) Real and imaginary parts of the effective index for different d_y, (b) Real and imaginary part of effective impedance. The same color convention as Fig. 4 is followed.

Figure 6 shows another interesting parameter, the ratio of the real and imaginary parts of n, which is a good indicator of the "quality" of the negative refraction. For thin metal lines along the electric field, the ratio is ~6, as d_y is increased, this quantity is shifted and reduced.

After both the effective refractive index and the impedance, ζ, are extracted, the effective permeability μ and permittivity ε can be simply calculated as $\mu = n\zeta$ and $\varepsilon = n/\zeta$, the real parts of which are shown in Fig.7. The maximum negative permeability decreases with the increase of the line width, which is due in part to the shrinking fill factor of the magnetic resonant structure; the absolute value of the effective permittivity increases with line width as the screening by the metal lines increases. The increasing $-\varepsilon$ compensates the decreasing $-\mu$, explaining the comparative stability of the maximum of $-n$. However, the impedance of the metamaterial is more mismatched to that of air with increasing d_y leading to a much smaller transmission.

From Figs. 5 and 7, the effective permeability of the sample with the largest d_y is barely negative over the range of negative refraction. This is very similar to the case in reference [8]; the negative refraction is mainly due to the real part of the permittivity and the imaginary part of the permeability. This is a high loss structure. For the sample with d_y=*100 nm*, over most of the range of negative refraction, both the real part of permeability and permittivity are negative, thus a double negative material with a dramatically lower loss is realized.

#7325 - $15.00 USD Received 29 April 2005; revised 10 June 2005; accepted 13 June 2005

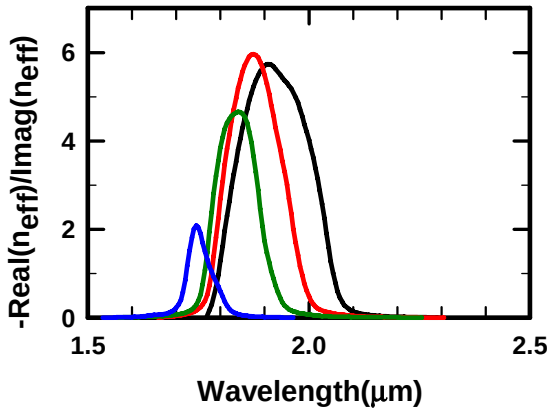

Fig. 6. Ratio of real and imaginary part of effective index for different d_y, The same color convention as fig. 4 is followed.

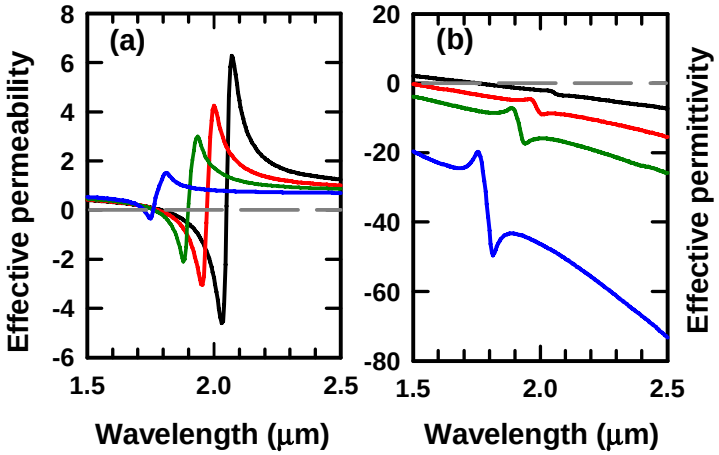

Fig. 7. (a) Real part of effective permeability (b) Real part of effective permittivity. The same color convention as fig. 4 is followed.

Next, we show that a simple Lorentz model nicely fits the simulation. In the Lorentz model, the permeability is expressed as [13,16]:

$$\mu(\omega) = \mu_\infty - \frac{f\omega_0^{\,2}}{\omega^2 - \omega_0^{\,2} + j\gamma\omega}, \tag{1}$$

here f is a fill factor and μ_∞ is the effective permeability for wavelengths far above the resonance. As shown in Ref. [17], a 2D array of holes in a metallic film $\mu_\infty \neq 0$, thus this parameter is estimated from the simulation results, and found to be around 0.6 for all the d_y parameters. As an example, in Fig. 9 we show the excellent fit of to the simulated permeability for d_y=*100 nm*, which has the strongest magnetic resonance.

Table 1 lists the extracted Lorentz parameters from Eq. (1) for different d_y. The fill factor f decreases from 0.2 to 0.045 as d_y is from 100- to 500-nm. The resonance frequency ω_∞ increases slightly with d_y (resonance wavelength λ_0 decreases), while the dissipation term γ increases by ~ 2. From Eq. (1), the strength of resonance is proportional to $f\omega_0/\gamma$, thus, the

#7325 - $15.00 USD Received 29 April 2005; revised 10 June 2005; accepted 13 June 2005

decreasing resonance strength with increasing d_y shown in Fig. 7 results from the decreasing fill factor and the increasing γ.

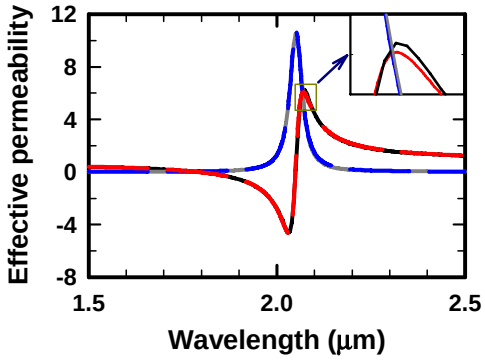

Fig. 8. Fit of the simulated effective permeability with a Lorentzian lineshape. Black and gray: RCWA simulation of the real and imaginary part of the permeability. Red and blue, the Lorentzian lineshape curve.

Table 1. Extracted parameters in equation (1)

d_y (nm)	f	ω_0(ev)	λ_0 (μm)	γ(ev)	$f\omega_0/\gamma$
100	0.201	0.605	2.05	0.0106	10.72
200	0.154	0.628	1.97	0.0136	6.93
300	0.112	0.651	1.90	0.0161	4.59
500	0.045	0.699	1.77	0.0198	1.57

4. Simulation with varying Au scattering loss

For the above simulation, bulk gold parameters are used. However, the electronic scattering parameter in thin Au films deposited by metal evaporation is typically larger than that of bulk gold. Here, we show that for the structures with thin metal wires along the electric field, even with the higher Au scattering frequency (~ 3×) found in previous experiments [8], simultaneous negative permittivity and permeability are still obtained.

In this section, we will fix the geometry of the structure, with d_x=500 nm and d_y=100 nm, and change the scattering loss of the Au film to 1-, 2- and 3-times that of bulk Au. Figure 9 (a) shows the real and imaginary parts of the effective index for the three different Au scattering parameters. On the short wavelength side of the resonance, which has the smaller imaginary part, the real part of the index decreases and the imaginary part increases. We plot again the quality factor, the ratio of the (- n_1) to n_2, in Fig. 9(b). The extremum of the ratio occurs at the same wavelength for the three scattering parameters, dropping from 6 to 2 as the scattering loss trebles. Nonetheless, for a considerable wavelength range, the ratio is larger than one.

Finally, the effective permeability and permittivity are extracted and shown in Fig. 10. Clearly, the impact of the scattering loss is mainly on the permeability, while the permittivity is only slightly effected. The range over which both the permeability and permittivity are negative corresponds to the negative refraction region in Fig. 9.

5. Summary

Following up the experimental work that has fabricated a negative index material in the near-IR [8], this paper systematically studies the effects of varying the geometry and scattering loss of the metal on the negative-index optical properties. The simulation results demonstrate that

#7325 - $15.00 USD Received 29 April 2005; revised 10 June 2005; accepted 13 June 2005

the NIM structure can be improved to exhibit simultaneous negative permeability and negative permittivity, i.e. to a double-negative material. In contrast to the work in Refs. [8, 9], the improved structure has a much lower loss, much better impedance matching, and thus a much higher transmission, which will lead to more extensive applications. Furthermore, the proposed structure has a minimum feature size of ~ 100 nm, and can be easily fabricated over a large-area sample by standard optical interferometric lithography techniques [18].

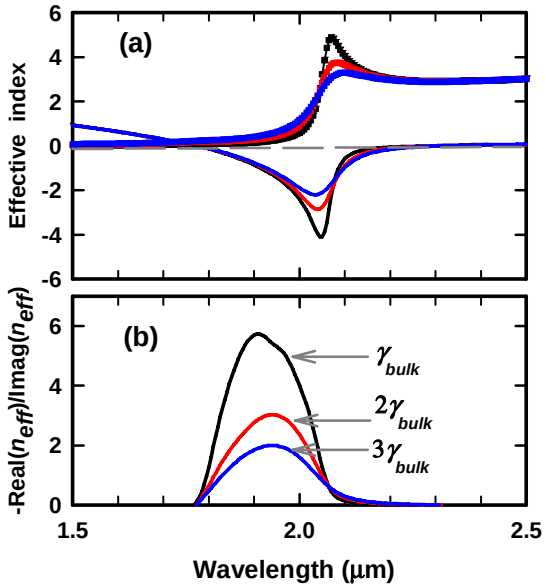

Fig. 9. (a) Effective index for scattering losses of 1- (black), 2- (red) and 3-times (blue) that of bulk Au. (b) Ratio of the real and imaginary parts of the index.

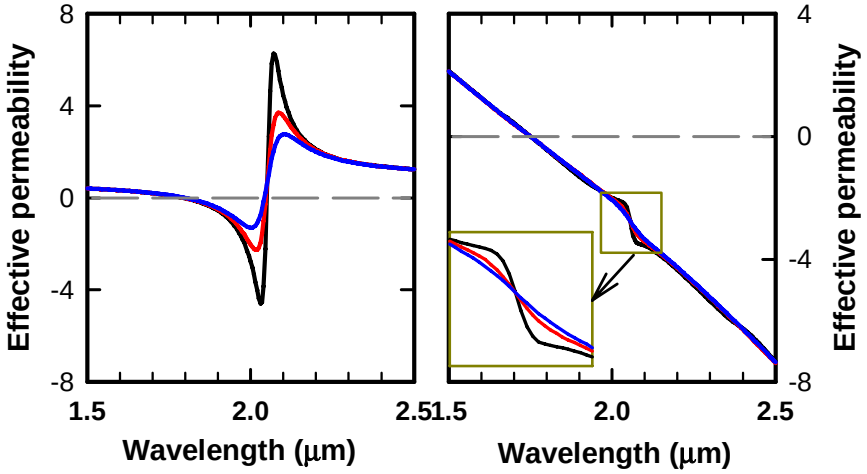

Fig. 10. (a) effective permeability and (b) effective permittivity for different scattering loss parameters of Au. The color convention in fig. 9 is followed.

#7325 - $15.00 USD
Received 29 April 2005; revised 10 June 2005; accepted 13 June 2005

Acknowledgments

This work was supported by DARPA under the University Photonics Research Center program.

#7325 - $15.00 USD Received 29 April 2005; revised 10 June 2005; accepted 13 June 2005